Vrije Universiteit Brussel

Structural basis for GABAA receptor potentiation by neurosteroids

Miller, Paul S; Scott, Suzanne; Masiulis, Simonas; De Colibus, Luigi; Pardon, Els; Steyaert, Jan; Aricescu, A Radu

nature
structural &
molecular biology

Structural basis for GABA$_A$ receptor potentiation by neurosteroids

Paul S Miller[1,5] , Suzanne Scott[1,2,5], Simonas Masiulis[1,2], Luigi De Colibus[1], Els Pardon[3,4] , Jan Steyaert[3,4] & A Radu Aricescu[1,2]

Type A γ-aminobutyric acid receptors (GABA$_A$Rs) are the principal mediators of inhibitory neurotransmission in the human brain. Endogenous neurosteroids interact with GABA$_A$Rs to regulate acute and chronic anxiety and are potent sedative, analgesic, anticonvulsant and anesthetic agents. Their mode of binding and mechanism of receptor potentiation, however, remain unknown. Here we report crystal structures of a chimeric GABA$_A$R construct in apo and pregnanolone-bound states. The neurosteroid-binding site is mechanically coupled to the helices lining the ion channel pore and modulates the desensitization-gate conformation. We demonstrate that the equivalent site is responsible for physiological, heteromeric GABA$_A$R potentiation and explain the contrasting modulatory properties of 3α versus 3β neurosteroid epimers. These results illustrate how peripheral lipid ligands can regulate the desensitization gate of GABA$_A$Rs, a process of broad relevance to pentameric ligand-gated ion channels.

GABA$_A$Rs are pentameric ligand-gated ion channels (pLGICs)[1]. Binding of the neurotransmitter GABA to the extracellular domain (ECD) opens an intrinsic pore surrounded by a ring of five M2 transmembrane domain (TMD) helices, one from each subunit, to permit the passage of negatively charged chloride ions[2]. The pore-opening event is subject to modulation by endogenous ligands such as Zn^{2+} and neurosteroids, including pregnanolone and its 5α epimer allopregnanolone[3]. Through their modulation of GABA$_A$Rs, neurosteroids are key regulators of the stress response and anxiety[4–6]. During the ovarian cycle, fluctuations in neurosteroid levels impact the GABA$_A$R inhibitory drive affecting neuronal excitability, thereby raising susceptibility to seizure and anxiety[7]. Changes to GABA$_A$R subunit expression levels in the dentate gyrus due to fluctuating neurosteroid concentrations are linked to postpartum depression following pregnancy[8]. Most GABA$_A$Rs in the human brain are heteromers, typically comprising two α subunits (α1–6), two β subunits (β1–3) and one γ (γ1–3) or δ subunit, out of 19 possible types[9]. The only GABA$_A$R structure solved to date, the β3 homopentamer crystallized in an agonist-bound desensitized conformation, offers the best available guide to a physiological receptor[10]. However, the other principal components of GABA$_A$Rs, the α subunits, are the components that convey neurosteroid potentiation through a key glutamine residue within the M1 helices[3,11]. In the absence of structural information, it is impossible to understand how neurosteroids modulate GABAergic neurotransmission in mechanistic terms. To address this limitation, we sought to express, characterize and solve structures of apo and neurosteroid-bound GABA$_A$R constructs containing α-subunit TMDs.

RESULTS

Neurosteroid potentiation of a β3–α5 chimeric GABA$_A$R

Heteromeric GABA$_A$Rs have, thus far, proved intransigent to structural determination, and α subunits expressed alone do not form homopentameric assemblies. To overcome these limitations, we generated a chimeric human receptor by fusing the α5-subunit TMD to the β3-subunit ECD. GABA$_A$R-β3 homopentamers are gated by the natural agonist histamine[10,12] (rather than GABA), and the chimera, referred to as α5$_{TMD}$, was also activated and then desensitized by histamine during whole-cell patch-clamp recordings from transfected HEK-293T cells (**Fig. 1a**). As reported for GABA$_A$R-β3 (ref. 12), α5$_{TMD}$ channels also mediate a picrotoxin-sensitive leak current (I_{PTX}) caused by spontaneous (agonist-independent) gating, which accounts for 67 ± 3% (n = 8 measurements) of the total current ($I_{histamineMAX}$ + I_{PTX}) (**Fig. 1b**). Thus, α5$_{TMD}$ assembles into a functional gating unit. To measure pregnanolone potentiation of submaximal histamine responses, it was necessary to reduce the high level of spontaneous activity in α5$_{TMD}$, because neurosteroids potentiate low-efficacy activated states, as observed in heteromeric GABA$_A$Rs[13]. To achieve this state, we introduced a point mutation, T287K, into the M2–M3 loop, which is critical for receptor gating (identified from screening residue swaps between the α5 and β3 subunits; see alignment in **Fig. 1c**), thereby reducing spontaneous gating from 67 ± 3% to 21 ± 3% (n = 16). On this background, pregnanolone strongly potentiated submaximal (EC$_{10–15}$) histamine doses by 325 ± 104%, n = 6 (EC$_{50}$ = 1.3 ± 0.1 μM, n = 6) (**Fig. 1d,e**). Notably, this effect was ablated by leucine substitution of the key M1 glutamine (α5 Gln245) previously identified to be essential for neurosteroid potentiation in heteromeric
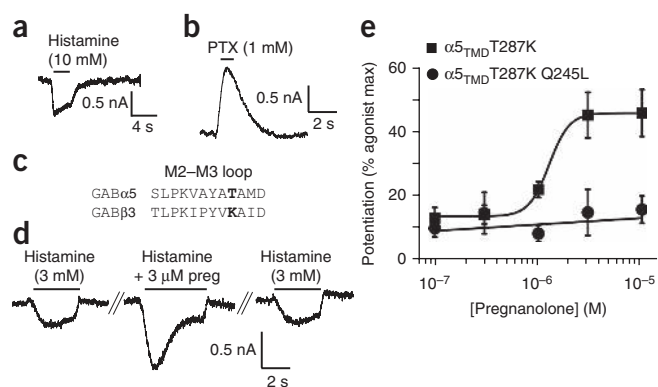
Figure 1 $\alpha5_{TMD}$ forms a functional gating unit potentiated by pregnanolone at the Gln245 site. (**a**) HEK-293T whole-cell patch-clamp recording of the agonist histamine activating an inward current through $\alpha5_{TMD}$ that subsequently desensitizes. (**b**) The classical $GABA_AR$ channel blocker picrotoxin blocks a spontaneous inward leak current generated by $\alpha5_{TMD}$. (**c**) Sequence alignment of the M2–M3 loop from $GABA_AR$ $\alpha5$ and $\beta3$ subunits, with T287K substitution bolded. (**d**) Raw whole-cell patch-clamp EC_{10} histamine responses from HEK cells transfected with $\alpha5_{TMD}T287K$, before and after coapplication with 3 µM pregnanolone (preg). (**e**) Pregnanolone dose–response curve for potentiation of histamine EC_{10-15} responses in $\alpha5_{TMD}T287K$ and the ablation of potentiation upon introduction of a Q245L mutation in the M1 helix. Each data point represents mean ± s.e.m. of $n = 6$ experiments, with each measurement from different cells. Source data for **e** are available online.

Table 1 Crystallographic data collection and refinement statistics

	Pregnanolone-bound $\alpha5_{TMD}$ (PDB 5O8F)	Apo $\alpha5_{TMD}$	
		Uncorrected	Anisotropy corrected (PDB 5OJM)
Data collection			
Space group	$I23$	$C2$	
Cell dimensions			
a, b, c (Å)	290.1, 290.1, 290.1	177.3, 139.9, 191.5	
α, β, γ (°)	90.0, 90.0, 90.0	90.0, 102.2, 90.0	
Resolution (Å)	205.13–3.15 (3.31–3.15)[a]	187.14–3.28 (3.42–3.28)	
R_{merge}	0.728 (3.107)	0.352 (2.807)	–
R_{meas}	0.741 (3.169)	0.371 (2.960)	–
R_{pim}	0.135 (0.621)	0.117 (0.936)	–
$I/\sigma(I)$	7.55 (1.26)	7.85 (1.08)	–
$CC_{1/2}$	0.988 (0.215)	0.998 (0.395)	–
Completeness (%)	99.94 (100.00)	99.78 (99.71)	–
Redundancy	30.4 (25.6)	10.0 (9.9)	–
Refinement			
Resolution (Å)	49.75–3.19 (3.31–3.19)	48.88–3.30 (3.42–3.30)	48.88–3.30 (3.42–3.30)
No. reflections	66,647 (6,629)	68,726 (6,866)	50,816 (473)
R_{work} / R_{free}	0.232 / 0.244 (0.360 / 0.367)	0.255 / 0.282 (0.389 / 0.395)	0.236 / 0.256 (0.244 / 0.261)
No. atoms			
Protein	18,217	–	18,141
N-linked glycans	485	–	397
Pregnanolone	115	–	–
B factors (Å²)			
Protein	72.1	–	71.3
N-linked glycans	90.7	–	99.1
Pregnanolone	59.6	–	–
R.m.s. deviations			
Bond lengths (Å)	0.008	–	0.009
Bond angles (°)	1.22	–	0.71

One crystal was used per structure. [a]Values in parentheses are for the highest-resolution shell.

$\alpha\beta\gamma/\delta$ $GABA_ARs$ (**Fig. 1e**). Furthermore, purified $\alpha5_{TMD}$ in detergent was thermostabilized by the addition of pregnanolone ($EC_{50} = 5.5 \pm 0.3$ µM, $n = 3$), and this thermostabilization was strongly attenuated by Q245L or Q245W mutations (tryptophan is the equivalent residue in $\beta1$–3 subunits) ($EC_{50} > 30$ µM, $n = 3$, in both cases) (**Supplementary Fig. 1**). Thus, whether in cell membranes or in detergent, $\alpha5_{TMD}$ houses a neurosteroid-potentiation site that requires the same key M1 glutamine to function as reported for heteromeric $GABA_ARs$.

The $\alpha5_{TMD}$ crystal structure

We next crystallized and determined the X-ray structures of $\alpha5_{TMD}$ in the absence and presence of pregnanolone to 3.3- and 3.2-Å resolution, respectively (**Table 1**, **Fig. 2a–d**, and **Supplementary Video 1**). In each case, $\alpha5_{TMD}$ was bound to a nanobody (Nb25) raised against the $\beta3$ ECD, which facilitated crystallization (**Supplementary Fig. 2a**). $\alpha5_{TMD}$ retains the hallmark architecture of all eukaryotic pLGICs characterized to date, including nicotinic acetylcholine, serotonin type 3, glycine and GluCl receptors[1,14–21]. Each subunit comprises an N-terminal $\beta3$ ECD folded into a twisted β-sandwich followed by an $\alpha5$ four-helical-bundle TMD (**Fig. 2a,b**). The principal face (P) of each subunit intercalates with the complementary face (C) of its neighbor to form a ring of five subunits surrounding a central vestibule at the ECD level, which flows into a five-fold pseudosymmetric pore in the TMD region. Each Nb25 straddles the neurotransmitter-binding site located under loop C between adjacent subunits (**Supplementary Fig. 2a–d**). The ECDs of the apo and pregnanolone-bound $\alpha5_{TMD}$ structures are very similar (r.m.s. deviation in the 0.16–0.21-Å range between different chains, over 204 equivalent Cα positions). Both structures adopt the same overall activated conformation as the agonist-bound $GABA_AR$-$\beta3$ (ref. 10), exhibiting a closed loop C that contrasts with the antagonist-bound open loop C in glycine receptors[16,17] (**Supplementary Fig. 2c,e,f**). When applied to $\alpha5_{TMD}$ T287K–transfected HEK-293T cells in whole-cell

patch-clamp recordings, Nb25 alone did not induce responses. Moreover, Nb25 did not affect maximal potentiation in the presence of 10 µM pregnanolone, the concentration used in crystallization experiments (**Supplementary Fig. 2g**). However, the activated state adopted by $\alpha5_{TMD}$ ECDs in crystal structures in the absence of agonist is consistent with the strong propensity of this construct to be spontaneously active in a cellular context (**Fig. 1b**).

Neurosteroid-binding modes

Surrounding the TMD pentamer of the pregnanolone-bound structure, but not the apo structure, five large peaks were observed in the $F_o – F_c$ omit electron density map. Each occupies a hydrophobic cavity at the interface between the principal M3 and complementary M1 helices of adjacent subunits (**Supplementary Fig. 3**). These densities were accounted for by pregnanolone molecules with half-chair geometry due to a *cis* junction between the A and B rings (**Fig. 2c,d**). The hydrophobic cavities contain the critical Gln245 residue, whose ε-oxygen contributes a putative hydrogen bond from the top of the
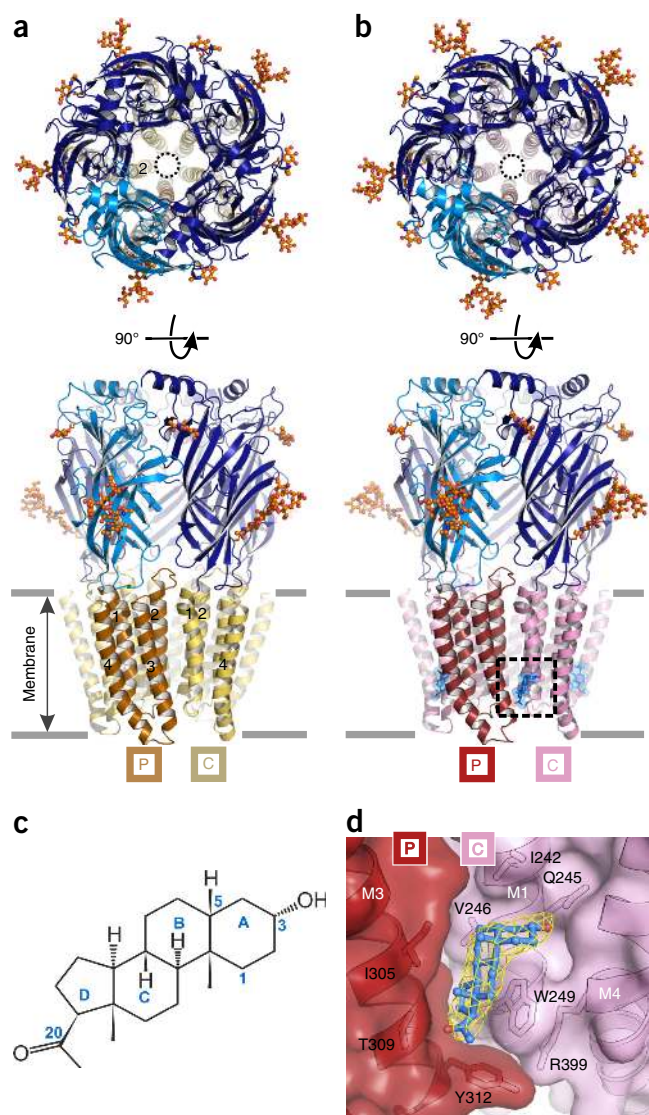
Figure 2 Architecture of GABA$_A$R $\alpha5_{TMD}$. Top-down (top) and side-on (bottom) views of the $\alpha5_{TMD}$ pentamer in apo (**a**) and pregnanolone-bound (**b**) forms. Subunits each comprise the $\beta3$ extracellular domain (dark and light blue) and $\alpha5$ TMD (α-helices M1–M4 shown in beige and yellow or red and pink). In top-down views, the pore is indicated by a black circle lined by five M2 helices (one per subunit). Side-on views highlight the helical organization (M1–M4, numbered 1–4 per subunit, where visible) in **a**, and the presence of pregnanolone in **b** (blue stick and space-fill, inside dashed box). N-linked glycans are shown as spheres colored by atom type (carbon atoms in orange, oxygen atoms in red). The principal (P) and complementary (C) subunits for the visible intersubunit interface are indicated. (**c**) Structural formula of pregnanolone with rings labeled A–D. Carbon atoms mentioned in the text are numbered. (**d**) Close-up of pregnanolone ('ball-and-stick' representation) bound to $\alpha5_{TMD}$ (cartoon and surface representation). The $2F_o - F_c$ electron density map surrounding the ligand is contoured at 1.3 σ (yellow mesh).

site to anchor the pregnanolone A ring 3α-hydroxyl (**Fig. 3a**). The neurosteroid A ring is positioned flat beneath the M1 Ile242 side chain, perpendicular to and above the indole rings of M1 Trp249 (**Fig. 3a**). The B–D rings angle downward, sandwiched between the side chains of M3 Ile305 and M1 Trp249. Tryptophan residues are highly prevalent in protein steroid-binding sites[22], and the stacking interaction observed is consistent with observations

from a previous study that showed that an aliphatic leucine substitution of this M1 tryptophan ablated potentiation in GABA$_A$R heteromers[11]. Pregnanolone B–D rings also make side-on van der Waals contacts with M1 Val246, which demarcates the deepest point of the pocket. Polar interactions anchor the neurosteroid at both ends. The D-ring C20 ketone anchors the bottom end of the ligand by acting as a hydrogen bond acceptor for the M3 Thr309 hydroxyl. Mutation of each of these residues individually, Q245S, V246A, W249L, I305A and T309A, all reduced sensitivity to pregnanolone potentiation of histamine responses on the T287K background by between three- and ten-fold, with W249L reducing sensitivity the most (from 0.8 ± 0.2 µM, $n = 4$ to > 10 µM, $n = 8$) and T309A reducing sensitivity the least (to 2.2 ± 0.3 µM, $n = 3$) (**Supplementary Fig. 4a**). Structural alignment of the $\beta3$ TMD pentamer[10] over the $\alpha5$ TMD pentamer and subsequent examination of α–β interfaces revealed that pregnanolone is well accommodated in the heteromer site at the β_P–α_C interface that contains the highly conserved α-subunit M1 glutamine (Gln245 in $\alpha5_{TMD}$, **Fig. 3b**). However, at the α_P–β_C interface, the equivalent M1 position is occupied by $\beta3$ Trp237, thus removing the potential for 3α-hydroxyl coordination, clashing with pregnanolone and closing the top of the pocket (**Fig. 3c,d**). Although no structure for the γ subunit is currently available, sequence alignment reveals an M1 tryptophan in place of M1 glutamine, suggesting that the α_P–γ_C pocket would be similarly occluded. Thus, $\alpha5_{TMD}$ possesses a neurosteroid-binding site that correctly predicts: (i) an involvement for the key M1 glutamine and tryptophan residues in heteromeric GABA$_A$Rs[3,11] and (ii) that receptor potentiation by neurosteroids only occurs via the β_P–α_C interface[23] (**Fig. 3b** versus **3c**).

A previous mutagenesis study, guided by homology modeling, had placed the α-subunit M1 glutamine close to M4 residues to create an intrasubunit pocket[3], rather than the intersubunit pocket described here. In $\alpha5_{TMD}$, the equivalent M4 residues Asn410 and Tyr413 are located outside the neurosteroid-binding site and are incompatible with ligand coordination by Gln245 (**Supplementary Fig. 4b,c**). Therefore, the previously reported effects of mutations to these residues on neurosteroid binding were, most likely, indirect. Moreover, $(3\alpha,5\beta)$-6-azipregnanolone photolabels $\beta3$ homopentameric GABA$_A$Rs at Phe301 (ref. 24), the residue equivalent to $\alpha5_{TMD}$ M3 Thr309 (**Fig. 3a,b**), consistent with the intersubunit site we identified. To functionally validate whether the neurosteroid-binding site observed crystallographically is equivalent to an intersubunit potentiation site in the heteromeric $\alpha1\beta3\gamma2$ GABA$_A$R, we introduced mutations into the β-subunit face that opposes the key heteromer α-subunit M1 glutamine and tryptophan residues[11]. We compared the sensitivity to pregnanolone potentiation of wild-type GABA$_A$R heteromers to those of heteromers containing $\beta3$ subunits with alanine substitutions at either M3 Leu297 (corresponding to $\alpha5_{TMD}$ Ile305) or M3 Phe301 (corresponding to $\alpha5_{TMD}$ Thr309) in whole-cell patch-clamp recordings from transfected HEK-293T cells (**Fig. 3e**). Both $\alpha1\beta3L297A\gamma2$ and $\alpha1\beta3F301A\gamma2$ GABA$_A$Rs retained wild-type-level sensitivity to the neurotransmitter GABA (wild-type (WT) EC$_{50}$ = 3.0 ± 1 µM, $n = 8$; L297A EC$_{50}$ = 5.0 ± 2 µM, $n = 3$; F301A EC$_{50}$ = 4.2 ± 2 µM, $n = 3$). However, $\alpha1\beta3L297A\gamma2$ GABA$_A$Rs were less sensitive to potentiation by both pregnanolone and its 5α epimer allopregnanolone (a *trans* isomer with a 'flat' geometry) by ten-fold and five-fold, respectively (pregnanolone WT EC$_{50}$ = 240 ± 20 nM, $n = 13$; L297A EC$_{50}$ = 2500 ± 200 nM, $n = 11$; allopregnanolone WT EC$_{50}$ = 280 ± 40 nM, $n = 5$; L297A EC$_{50}$ = $1,600 \pm 200$ nM, $n = 9$) (**Fig. 3e,f**). In contrast, $\alpha1\beta3F301A\gamma2$ GABA$_A$Rs retained wild-type-level sensitivity to both pregnanolone and allopregnanolone potentiation (pregnanolone EC$_{50}$
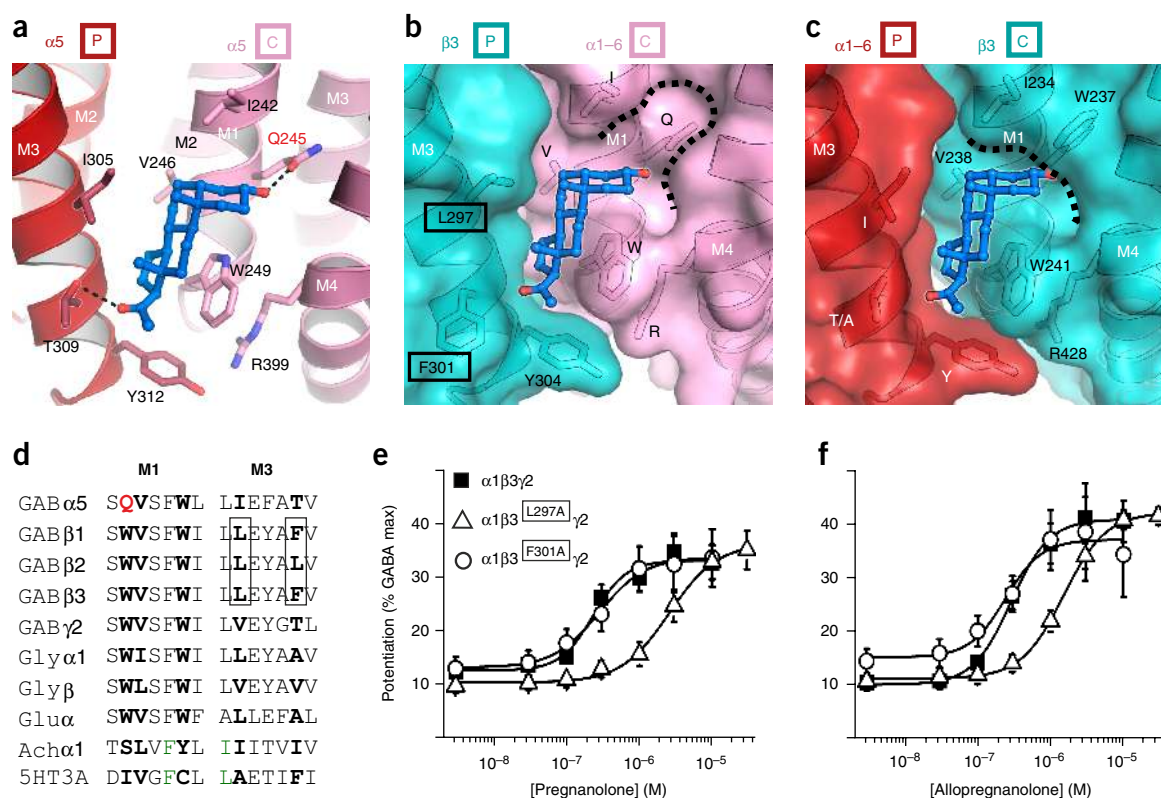
Figure 3 The neurosteroid potentiation site. (**a**) Pregnanolone (ball-and-stick representation; carbon atoms in blue, oxygen atoms in red) bound to an intersubunit site between M3 residues on the P face of one subunit and M1 residues on the C face of the next. Putative hydrogen bonds between the pregnanolone 3α-hydroxyl and the Gln245 amide (2.4 Å) and the C20 ketone and Thr309 hydroxyl (3.0 Å) are indicated by dashed lines. (**b,c**) Modeled heteromeric β_P–α_C (**b**) and α_P–β_C (**c**) interfaces in cartoon and surface representation, in which the relevant $\alpha5_{TMD}$ face is substituted by the equivalent β3 subunit structure (PDB 4COF). Note that the α5 residues in these two panels are labeled by letters only, without numbers, to reflect their conservation across the α subunits (α1–6) within this site. Pregnanolone is well accommodated in the heteromeric β_P–α_C site (**b**) but not in the α_C–β_P site (**c**) owing to the replacement of the α-subunit M1 glutamine with the β3 M1 Trp237, which closes the top of the pocket (dashed line). (**d**) Sequence alignment of the M1 and M3 motifs containing the neurosteroid-binding-site residues (bold) in the GABA$_A$R α5 subunit and equivalent regions in other human pLGIC superfamily members. M1 Gln245, unique to GABA$_A$R α subunits, is highlighted in red. GABA$_A$R β-subunit residues contributed from the complementary face in heteromeric receptors are boxed. (**e**) Pregnanolone and (**f**) allopregnanolone dose–response curves for potentiation of GABA EC_{10-15} responses. Alanine substitution of the β3 principal-face residue Leu297, but not Phe301, reduces neurosteroid sensitivity. These residues are highlighted by black boxes in **b**. Each data point represents mean ± s.e.m. Pregnanolone EC_{50}: WT, $n = 13$; L297A, $n = 11$; F301A, $n = 8$. Allopregnanolone EC_{50}: WT, $n = 5$; L297A, $n = 9$; F301A, $n = 4$. Each measurement is from different cells. Source data for **e** and **f** are available online.

$= 280 \pm 40$ nM, $n = 8$; allopregnanolone $EC_{50} = 260 \pm 60$ nM, $n = 4$). This finding is consistent with Phe301 having a more distal location on the border of the pocket, as well as with its lack of conservation between human β-subunit subtypes at this position and the fact that the β-subunit subtype does not impact neurosteroid potentiation[25]. However, the strong impact of the β3 L297A mutation confirms that the intersubunit location of the neurosteroid site observed in $\alpha5_{TMD}$ is retained in α1β3γ2 heteromeric GABA$_A$Rs.

To explore the $\alpha5_{TMD}$ neurosteroid-binding mechanism further, we performed *in silico* analyses using the quantum mechanics polarized ligand docking (QMPLD)[26] algorithm implemented in the Schrödinger suite (http://www.schrodinger.com). The binding mode observed upon pregnanolone docking into the $\alpha5_{TMD}$ neurosteroid pocket was in agreement with the crystal structure (r.m.s. deviation of 1.7 Å, calculated by VMD over all pregnanolone atoms) (**Fig. 4a** and **Supplementary Fig. 5a**). Van der Waals contacts were predicted to be the predominant driving force of interaction (binding energy of −36.6 kcal mol⁻¹), consistent with other steroid-binding site analyses[27]. The electrostatic contribution was only −1.2 kcal mol⁻¹. Despite an elongated flat geometry rather than half-chair geometry,

allopregnanolone was also well accommodated into the site (**Fig. 4b**), with a similar binding energy ($E_{vdw} = -35.4$ kcal mol⁻¹; $E_{coul} = -1.4$ kcal mol⁻¹). Moreover, pregnanolone and allopregnanolone similarly potentiated the $\alpha5_{TMD}$T287K histamine responses (**Supplementary Fig. 5b**). Allopregnanolone retained the same binding mode for its 3α-hydroxyl, positioned equidistantly between the M1 Gln245 εO and the Trp249 εN (3.5 Å for pregnanolone; 3.6 Å for allopregnanolone). Owing to its elongated flat geometry, binding imposed a 1.2-Å downward translation on the allopregnanolone B–D rings. In contrast to pregnanolone, its 3β epimer epipregnanolone is a weak potentiator of GABA$_A$R heteromers[28]. Epipregnanolone has been shown to noncompetitively antagonize pregnanolone potentiation, thus raising the hypothesis that it acts through an alternative site[28]. However, our epipregnanolone docking in the $\alpha5_{TMD}$ neurosteroid pocket led to similar binding energy estimates ($E_{vdw} = -35.5$ kcal mol⁻¹; $E_{coul} = -1.8$ kcal mol⁻¹), suggesting that it can bind the same site as pregnanolone and allopregnanolone. These alternative scenarios can be reconciled if epipregnanolone binding to one GABA$_A$ heteromer site allosterically prevents potentiation by pregnanolone bound at the other. However, the possibility also remains that GABA$_A$R heteromers contain
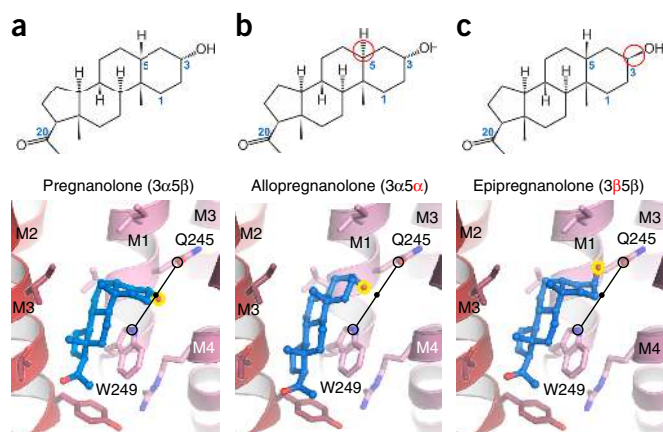
Figure 4 Computational docking of pregnanolone and related neurosteroids. Structural formulae and $\alpha5_{TMD}$ structures showing binding modes of computationally docked pregnanolone (**a**), allopregnanolone (**b**) and epipregnanolone (**c**). Stereoisomeric differences from pregnanolone are indicated in formulae by red circles. In the 3D models, the critical C3 hydroxyl group is highlighted by a yellow circle. Potentiators possess a 3α-hydroxyl, which is docked equidistantly between the Gln245 εO and Trp249 εN (3.5 Å for pregnanolone; 3.6 Å for allopregnanolone; indicated by a solid black line) regardless of whether the rings assume a half-chair or flat geometry. The C3 hydroxyl of 3β pregnanolone can only share a putative hydrogen bond with the Gln245 amide (2.8-Å distance).

additional, nonoverlapping sites that bind epipregnanolone and mediate noncompetitive inhibition. Notably, our docking studies reveal that the 3α-hydroxyl group of epipregnanolone points 'upward' rather than 'downward', thereby losing potential coordination with the Trp249 εN, although potential coordination with Gln245 εO is retained (**Fig. 4c**). We propose that the positioning of the 3α-hydroxyl between the Gln245 and Trp249 side chains is a contributing factor in determining whether transduction is potentiating or inhibitory in GABA$_A$R heteromers. In contrast to its very weak potentiation on GABA$_A$R heteromers, epipregnanolone triggers significant $\alpha5_{TMD}$T287K potentiation (**Supplementary Fig. 5b**). This might be due to its cumulative action through the five neurosteroid-binding sites present in $\alpha5_{TMD}$T287K, as opposed to that through only two equivalent sites in GABA$_A$R heteromers, thus resulting in a stronger effect. Nevertheless, in these circumstances, the proposal that an 'upward' position of the 3α-hydroxyl reduces neurosteroid potentiation cannot be validated in the $\alpha5_{TMD}$T287K chimera.

Impact of neurosteroid binding on TMD conformation

To examine the impact of pregnanolone binding on the pore conformation, we next compared the TMD regions of the apo and pregnanolone-bound $\alpha5_{TMD}$ structures. Individual subunit TMDs closely superimpose (r.m.s. deviation in the 0.43–0.55-Å range between different chains over 123 equivalent Cα positions), adopting pore conformations similar to that of the desensitized GABA$_A$R-β3 homopentamer[10] (**Fig. 5a**), rather than to the open, desensitized (or partly open) and closed conformations of the related glycine receptor (GlyR)[16,17] (**Fig. 5b**). In both apo and pregnanolone-bound states, the five M2 helices lining the pore, taper inward to a constriction at the intracellular end. The side chains of Val260 and Pro256, occupying the 2′ and −2′ positions (pLGIC pore numbering convention), demarcate a hydrophobic desensitization gate (**Fig. 5a**). However, whereas the pore diameter at 2′ valine appears to be state independent (4.8 Å), pregnanolone binding leads to pore enlargement, from 3.7-Å
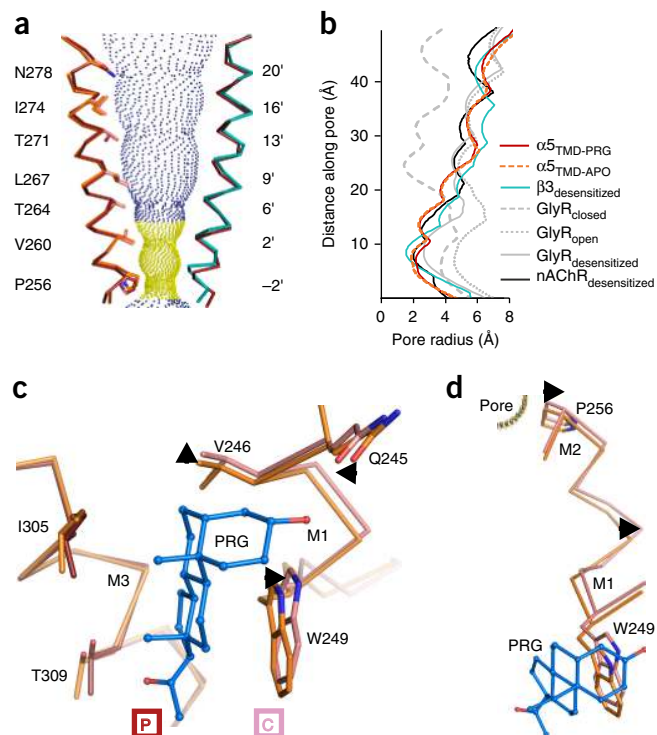

Figure 5 Pore conformation and neurosteroid-induced motions in $\alpha5_{TMD}$. (**a**) View of two opposing pore-lining M2 helices, the other three being removed for clarity. The pregnanolone-bound $\alpha5_{TMD}$ state (red) is shown on both sides. For comparison, overlays of the $\alpha5_{TMD}$ apo state (left, orange) and of GABA$_A$R-β3 (right, teal) M2 helices are shown. Blue and yellow spheres define pregnanolone-bound $\alpha5_{TMD}$ pore radii greater than or less than 3.2 Å, respectively (the radius of a hydrated Cl$^-$ ion). (**b**) A plot of pore radii for $\alpha5_{TMD}$ structures compared to GABA$_A$R-β3 in the desensitized state (PDB 4COF), the glycine receptor in the resting closed, open and desensitized states (PDB 5JAD, PDB 5JAE and PDB 5JAF) and $\alpha4\beta2$ nAChR (PDB 5KXI). (**c**) Superposition of apo (orange) versus pregnanolone-bound (red) $\alpha5_{TMD}$ principal faces reveals pregnanolone-induced motions on the complementary face (pink) of the neurosteroid pocket (indicated by black arrowheads). (**d**) The same superposition as in **c**, zoomed in on the pregnanolone-induced motions along the M1–M2 linker of a complementary face subunit, which impact the Pro256 desensitization gate.

to 4.3-Å diameter, at −2 proline (**Fig. 5b** and **Supplementary Video 2**). This contrasts with the GABA$_A$R-β3 homopentamer, in which the desensitization gate comprises only a single ring at −2′ (Ala248) with a 3.1-Å diameter (**Supplementary Fig. 6**), but is reminiscent of the cation-conducting $\alpha4\beta2$ nicotinic acetylcholine receptor (nAChR) in which two rings of residues at 2′ and −1′ form a similar, albeit negatively charged, gate[21] (**Fig. 5b**). Although the $\alpha5_{TMD}$ pore in both states is theoretically wide enough to conduct dehydrated Cl$^-$ ions (Pauling radius 1.8 Å), the gate contains no polar groups to substitute for the hydration shell and is highly likely to impede conductance[29].

The increased −2′ proline-ring diameter is the result of neurosteroid pocket expansion, required to accommodate pregnanolone (**Fig. 5c,d** and **Supplementary Video 2**). Neurosteroid binding displaces the complementary face away from the principal face, in particular at M1 Val246 (Cα displaced 0.9 Å) and Trp249 (Cα displaced 0.7 Å). Contrasting with this expansion, the polar interaction from the 3α-hydroxyl draws the side chain of Gln245 into the pocket by 0.6 Å and down toward the Trp249 εN by 0.7 Å (measurements
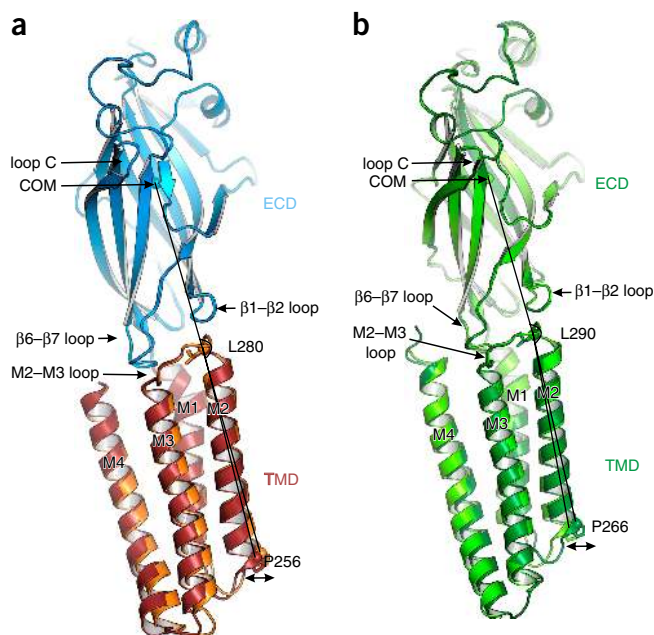
Figure 6 TMD motions relative to the ECD. (**a**) Side-on view of a single subunit (B chains), from apo α5$_{TMD}$ (orange TMD) and pregnanolone-bound α5$_{TMD}$ (red TMD), superposed by their ECDs (blue). The ECD conformations are very similar (r.m.s. deviation of 0.19 Å over 204 equivalent Cα positions). However, the lower half of the pregnanolone-bound TMD flexes such that the desensitization gate at Pro256 swings outward from the pore (indicated by double-headed arrow). The angles measured between the ECD center of mass (COM) and the Cα atoms of Leu280 at the top of M2 and Pro256 at the bottom of M2 are 162.5° (apo α5$_{TMD}$) and 164.4° (pregnanolone-bound α5$_{TMD}$), respectively, and thus, a 1.9° swing. (**b**) Equivalent view and superposition between open GlyR (light green, PDB 3JAE) and desensitized (or partially open) GlyR (dark green, PDB 3JAF). The narrowest pore diameter is at –2′ (Pro266) position in both cases (8.8 Å and 5 Å, respectively). The GlyR ECD conformations are also very similar (r.m.s. deviation of 0.31 Å over 210 equivalent Cα positions in B chains). As observed in α5$_{TMD}$, relative to the superimposed ECDs, the lower half of the GlyR TMD flexes such that the desensitization gate at Pro266 is displaced outward from the pore to expand and open the channel. The angles measured between the ECD COM and the Cα atoms of Leu290 at the top of M2 and Pro266 at the bottom of M2 are 161.4° (desensitized GlyR) and 164.1° (open GlyR), respectively, and thus, a 2.7° swing.

corresponding to Gln245 εO in both cases). The resultant torque from this rearrangement at the base of the M1 helix, which twists sideways and outward, drives the translation of the M1–M2 intracellular linker (**Fig. 5d** and **Supplementary Video 2**; mean Cα displacement of Leu250, Asn251, Arg252, Glu253, Ser254, Val255 is 0.95 Å), which is not involved in crystal packing (**Supplementary Fig. 7**).

Aside from pore dilation, which partly relieves its hydrophobic constriction, pregnanolone binding has longer-range effects that extend upward through the TMD helical bundles and destabilize their desensitized-state arrangement. Notably, straightening of the M2 helices drives their extracellular ends and the contiguous M2–M3 loop (a key component of the TMD–ECD interface) inward (**Supplementary Video 3**). This shift leads to an overall straightening of the subunits, with the ECD and TMD undergoing a rocking motion about their shared interface as α5$_{TMD}$ switches between apo and pregnanolone-bound states (**Fig. 6a** and **Supplementary Video 3**). The type and magnitude of motions observed here are consistent with those previously proposed to support transitions between gating

states in the heteromeric *Torpedo* nAChR, studied within a membrane environment[30], as well as in the detergent-solubilized homopentameric zebrafish α1 GlyR[16] (**Fig. 6b**) and *Caenorhabditis elegans* GluClα receptor[19], suggesting that all these constructs operate in the same allosteric framework, which is broadly applicable to pLGICs[1].

The observed outward pull on the desensitization gate in response to binding pregnanolone and the impact of structure-guided mutagenesis offer a molecular mechanism by which neurosteroids support pore opening in heteromeric receptors. Consistent with this model, the M1–M2 linker controls desensitization in heteromeric GABA$_A$Rs[31]. Expansion of the TMD intersubunit space as a mechanism of potentiation has previously been described for the antiparasitic agent ivermectin binding to the related *C. elegans* receptor GluCl (refs. 18,19). However, ivermectin binds GluCl to a pocket higher up the TMD that is not observed in GABA$_A$Rs and penetrates deeper between the subunits (**Supplementary Fig. 8a,b**).

DISCUSSION

Here, we present structures of the homomeric GABA$_A$R construct α5$_{TMD}$ in apo form and bound to a potentiation site by the endogenous neurosteroid pregnanolone. The binding site for neurosteroids corresponds to the site in heteromeric αβγ/δ GABA$_A$Rs, which constitute the vast majority of physiological GABA$_A$Rs[9]. These structures reveal the mode of neurosteroid binding and the motions induced in response to binding. Pregnanolone binds at the intersubunit interface between the M3 helix on the principal face and the M1 helix on the complementary face. Consistent with the high hydrophobicity of neurosteroids, binding is driven by interactions with hydrophobic residues (–36.6 kcal mol^{-1} of the total –37.8 kcal mol^{-1} binding energy), in particular by a stacking interaction between the pregnanolone B–D rings and the α5 M1 Trp249. The critical M1 Gln245 residue forms a putative hydrogen bond via its ε-oxygen to the pregnanolone A ring 3α-hydroxyl. Expansion of Trp249 away from M3 to accommodate pregnanolone within the site, combined with attraction of Gln245 toward pregnanolone stacked on Trp249 imparts torque on the lower segment of M1, which triggers a sideways motion on the M1–M2 linker and withdraws M2 at the –2 ring to expand the desensitization gate. The structure of the α5$_{TMD}$ homopentamer potentiation site, compared with that of GABA$_A$R-β3 (ref. 10), also explains why in heteromeric GABA$_A$Rs neurosteroids are well accommodated at the two β$_P$–α$_C$ interfaces (**Fig. 3a–c**) but not at the two α$_P$–β$_C$ interfaces[23]. In the latter, the key α$_C$ M1 Gln245 is replaced by β$_C$ Trp237, which occludes the site and sterically clashes with the neurosteroid.

In a physiological context, extrasynaptic GABA$_A$Rs are key targets for endogenous neurosteroids[32]. In particular, neurosteroids increase tonic inhibition by promoting the opening of GABA$_A$Rs that are only partially occupied by the low ambient concentrations of GABA present in the extrasynaptic regions[32]. The structural framework provided by α5$_{TMD}$ in a desensitized state, bound by pregnanolone, reveals that the molecular basis of this physiological process can be accounted for by the neurosteroid drawing the equilibrium away from the closed resting state toward open and desensitized states. The degree by which neurosteroid binding supports the open state versus the desensitized state probably depends on the surrounding lipid environment. Neurosteroids potentiated the open state of α5$_{TMD}$ in whole-cell patch-clamp recordings in HEK cells, within a membrane environment, but was bound to desensitized α5$_{TMD}$ in detergent micelles in the crystal structure. The α5$_{TMD}$ structure also reveals the exposed location of the neurosteroid site on the outer face of the TMD, meaning that pregnanolone will bridge interactions

between the GABA$_A$R and the lipid bilayer. Thus, it is not surprising that the broader lipidic context of the protein will affect the extent to which neurosteroid binding expands the desensitization gate and so potentiates the open state.

Overall, this study provides key insights into the mechanical coupling between peripheral lipid-binding sites and the channel desensitization gate and illustrates a novel form of modulation within the pLGIC superfamily.

METHODS

Methods, including statements of data availability and any associated accession codes and references, are available in the online version of the paper.

Note: Any Supplementary Information and Source Data files are available in the online version of the paper.

AUTHOR CONTRIBUTIONS

Experimental work was performed by P.S.M. and S.S. (protein expression, purification, crystallization, electrophysiology), S.M. (protein expression, purification), L.D.C. (docking experiments), E.P. and J.S. (nanobody generation) and A.R.A. (crystallography). The manuscript was written by P.S.M. and A.R.A. with input from all coauthors.

COMPETING FINANCIAL INTERESTS

The authors declare no competing financial interests.

1. Nemecz, Á., Prevost, M.S., Menny, A. & Corringer, P.J. Emerging molecular mechanisms of signal transduction in pentameric ligand-gated ion channels. *Neuron* **90**, 452–470 (2016).
2. Miller, P.S. & Smart, T.G. Binding, activation and modulation of Cys-loop receptors. *Trends Pharmacol. Sci.* **31**, 161–174 (2010).
3. Hosie, A.M., Wilkins, M.E., da Silva, H.M. & Smart, T.G. Endogenous neurosteroids regulate GABAA receptors through two discrete transmembrane sites. *Nature* **444**, 486–489 (2006).
4. Majewska, M.D., Harrison, N.L., Schwartz, R.D., Barker, J.L. & Paul, S.M. Steroid hormone metabolites are barbiturate-like modulators of the GABA receptor. *Science* **232**, 1004–1007 (1986).
5. Sarkar, J., Wakefield, S., MacKenzie, G., Moss, S.J. & Maguire, J. Neurosteroidogenesis is required for the physiological response to stress: role of neurosteroid-sensitive GABAA receptors. *J. Neurosci.* **31**, 18198–18210 (2011).
6. Gunn, B.G., Brown, A.R., Lambert, J.J. & Belelli, D. Neurosteroids and GABA(A) Receptor Interactions: A Focus on Stress. *Front. Neurosci.* **5**, 131 (2011).
7. Maguire, J.L., Stell, B.M., Rafizadeh, M. & Mody, I. Ovarian cycle-linked changes in GABA(A) receptors mediating tonic inhibition alter seizure susceptibility and anxiety. *Nat. Neurosci.* **8**, 797–804 (2005).
8. Maguire, J. & Mody, I. GABA(A)R plasticity during pregnancy: relevance to postpartum depression. *Neuron* **59**, 207–213 (2008).
9. Sigel, E. & Steinmann, M.E. Structure, function, and modulation of GABA(A) receptors. *J. Biol. Chem.* **287**, 40224–40231 (2012).
10. Miller, P.S. & Aricescu, A.R. Crystal structure of a human GABAA receptor. *Nature* **512**, 270–275 (2014).
11. Akk, G. *et al.* Mutations of the GABA-A receptor alpha1 subunit M1 domain reveal unexpected complexity for modulation by neuroactive steroids. *Mol. Pharmacol.* **74**, 614–627 (2008).
12. Saras, A. *et al.* Histamine action on vertebrate GABAA receptors: direct channel gating and potentiation of GABA responses. *J. Biol. Chem.* **283**, 10470–10475 (2008).
13. Bianchi, M.T. & Macdonald, R.L. Neurosteroids shift partial agonist activation of GABA(A) receptor channels from low- to high-efficacy gating patterns. *J. Neurosci.* **23**, 10934–10943 (2003).
14. Hassaine, G. *et al.* X-ray structure of the mouse serotonin 5-HT3 receptor. *Nature* **512**, 276–281 (2014).
15. Miyazawa, A., Fujiyoshi, Y. & Unwin, N. Structure and gating mechanism of the acetylcholine receptor pore. *Nature* **423**, 949–955 (2003).
16. Du, J., Lü, W., Wu, S., Cheng, Y. & Gouaux, E. Glycine receptor mechanism elucidated by electron cryo-microscopy. *Nature* **526**, 224–229 (2015).
17. Huang, X., Chen, H., Michelsen, K., Schneider, S. & Shaffer, P.L. Crystal structure of human glycine receptor-α3 bound to antagonist strychnine. *Nature* **526**, 277–280 (2015).
18. Althoff, T., Hibbs, R.E., Banerjee, S. & Gouaux, E. X-ray structures of GluCl in apo states reveal a gating mechanism of Cys-loop receptors. *Nature* **512**, 333–337 (2014).
19. Hibbs, R.E. & Gouaux, E. Principles of activation and permeation in an anion-selective Cys-loop receptor. *Nature* **474**, 54–60 (2011).
20. Unwin, N. Refined structure of the nicotinic acetylcholine receptor at 4A resolution. *J. Mol. Biol.* **346**, 967–989 (2005).
21. Morales-Perez, C.L., Noviello, C.M. & Hibbs, R.E. X-ray structure of the human α4β2 nicotinic receptor. *Nature* **538**, 411–415 (2016).
22. Hori-Tanaka, Y., Yura, K., Takai-Igarashi, T. & Tanaka, H. Structural classification of steroid-binding sites on proteins by coarse-grained atomic environment and its correlation with their biological function. *Steroids* **96**, 81–88 (2015).
23. Bracamontes, J.R., Li, P., Akk, G. & Steinbach, J.H. A neurosteroid potentiation site can be moved among GABAA receptor subunits. *J. Physiol. (Lond.)* **590**, 5739–5747 (2012).
24. Chen, Z.W. *et al.* Neurosteroid analog photolabeling of a site in the third transmembrane domain of the β3 subunit of the GABA(A) receptor. *Mol. Pharmacol.* **82**, 408–419 (2012).
25. Belelli, D., Casula, A., Ling, A. & Lambert, J.J. The influence of subunit composition on the interaction of neurosteroids with GABA(A) receptors. *Neuropharmacology* **43**, 651–661 (2002).
26. Cho, A.E., Guallar, V., Berne, B.J. & Friesner, R. Importance of accurate charges in molecular docking: quantum mechanical/molecular mechanical (QM/MM) approach. *J. Comput. Chem.* **26**, 915–931 (2005).
27. Eick, G.N. & Thornton, J.W. Evolution of steroid receptors from an estrogen-sensitive ancestral receptor. *Mol. Cell. Endocrinol.* **334**, 31–38 (2011).
28. Wang, M. *et al.* 3beta-hydroxypregnane steroids are pregnenolone sulfate-like GABA(A) receptor antagonists. *J. Neurosci.* **22**, 3366–3375 (2002).
29. Aryal, P., Sansom, M.S. & Tucker, S.J. Hydrophobic gating in ion channels. *J. Mol. Biol.* **427**, 121–130 (2015).
30. Unwin, N. & Fujiyoshi, Y. Gating movement of acetylcholine receptor caught by plunge-freezing. *J. Mol. Biol.* **422**, 617–634 (2012).
31. Gielen, M., Thomas, P. & Smart, T.G. The desensitization gate of inhibitory Cys-loop receptors. *Nat. Commun.* **6**, 6829 (2015).
32. Brickley, S.G. & Mody, I. Extrasynaptic GABA(A) receptors: their function in the CNS and implications for disease. *Neuron* **73**, 23–34 (2012).

ONLINE METHODS

Construct design. The $\alpha5_{TMD}$ construct was designed by fusing the ECD of the human $GABA_AR$ β3 subunit (mature polypeptide numbering 1–217, QSVN… LKRN; Uniprot P28472) to the TMD of the human $GABA_AR$ α5 subunit (mature polypeptide numbering 226–431, IGYF…GAASPK; Uniprot P31644). The α5 intracellular M3–M4 loop amino acids 316–392 (RGWA…NSIS) were substituted by the SQPARAA sequence[10,33] to enhance the recombinant protein yield and facilitate crystallization. This construct was cloned into the pHLsec vector[34] between the N-terminal secretion signal sequence and a the C-terminal 1D4 purification tag derived from bovine rhodopsin (TETSQVAPA), which is recognized by the Rho-1D4 monoclonal antibody (University of British Columbia)[35,36]. Point mutations were introduced to constructs by overlap PCR of whole-construct cDNAs and subsequent ligation into the pHLsec vector[34].

Large-scale expression and purification of $\alpha5_{TMD}$. 20-L batches of HEK293S-GnTI⁻ cells (ATCC Cat# CRL-3022, RRID: CVCL_A785), which yield proteins with truncated N-linked glycans, $Man_5GlcNAc_2$ (refs. 37,38), were grown in suspension to densities of 2×10^6 cells ml⁻¹ in Protein Expression Media (PEM, Invitrogen) supplemented with L-glutamine, nonessential amino acids (Gibco) and 1% fetal calf serum (Sigma-Aldrich) in 200-ml volumes, each in empty 600-ml DMEM bottles (Gibco) with lids loose, shaking at 130 r.p.m., 37 °C, 8% CO_2. For transient transfection, cells from 1 L of culture were collected by centrifugation (200g for 5 min) and resuspended in 150 ml Freestyle medium (Invitrogen) containing 3 mg PEI Max (Polysciences) and 1 mg plasmid DNA, and then incubated for 4 h in a 2-L conical flask with shaking at 160 r.p.m. Subsequently, culture media were topped up to 1 L with PEM containing 1 mM valproic acid and returned to empty DMEM bottles. Typically, 40–70% transfection efficiencies were achieved, as assessed using control transfections with a monoVenus-expressing plasmid[39,40]. 72 h post-transfection cell pellets were collected, snap frozen in liquid N_2 and stored at −80 °C.

Cell pellets (~200 g) were solubilized in 600 ml buffer containing 20 mM HEPES, pH 7.2, 300 mM NaCl, 1.5% (w/v) dodecyl 1-thio-β-maltoside (DDTM, Anatrace), 1% (v/v) mammalian protease inhibitor cocktail (Sigma-Aldrich, cat. P8340) for 2 h at 4 °C. Insoluble material was removed by centrifugation (10,000g, 15 min). The supernatant was diluted two-fold in a buffer containing 20 mM HEPES, pH 7.2, and 300 mM NaCl and incubated for 2 h at 4 °C with 10 ml CNBr-activated Sepharose beads (GE Healthcare) precoated with 50 mg Rho-1D4 antibody (3.3 g dry powdered beads expand during antibody coupling to approximately 10 ml). Affinity-bound samples were washed slowly by gravity flow over 2 h at 4 °C with 200 ml of buffer containing 20 mM HEPES, pH 7.2, 300 mM NaCl and 0.1% (w/v) DDTM (approximately 20× CMC) and then 200 ml of buffer containing 20 mM HEPES, pH 7.2, 300 mM NaCl and 0.01% (w/v) DDTM. $\alpha5_{TMD}$ was eluted overnight in 15 ml of buffer containing 15 mM HEPES, pH 7.2, 225 mM NaCl, 0.007% (w/v) DDTM and 500 μM TETSQVAPA peptide (Genscript). The eluate was centrifuged (30,000g, 15 min) and the supernatant was concentrated by ultrafiltration to 1–2 ml at 1–5 mg/ml using 100-kDa-cutoff membranes (Millipore). The concentrated sample was centrifuged (30,000g, 15 min) and the supernatant was aliquoted in 0.5–1.5 mg protein per 0.7 ml aliquots and either snap frozen for storage at −80 °C or gel filtrated as appropriate. A single aliquot was loaded onto a Superose 6 10/300 Increase gel filtration column (GE Healthcare) equilibrated in 10 mM HEPES, pH 7.2, 150 mM NaCl and 0.007% (w/v) DDTM. The nanobody Nb25, expressed and purified as described below, was added to $\alpha5_{TMD}$ at ten-fold molar excess and the complex was concentrated by ultrafiltration to 4 mg/ml, using a 100-kDa-cutoff membranes (Millipore) for crystallization trials. Typical final yields were 0.2 mg $\alpha5_{TMD}$ per liter of cells grown in suspension (10g cell pellet). For the production of neurosteroid-bound $\alpha5_{TMD}$, the gel filtration buffer described above was supplemented with pregnanolone, 30 μM final concentration.

Large-scale expression and purification of heteromeric α1β3 $GABA_ARs$ for generation of nanobody libraries. Human $GABA_AR$ α1 and β3 subunits wild-type mature protein sequences were used (α1 Uniprot P14867 entry Gln28 is Gln1 1–429 QPSL…PTPHQ; β3 Uniprot P28472 isoform 1 entry Gln26 is Gln1 1–448 QVSN…LYYVN), except that the intracellular loop between transmembrane helices 3 and 4 (M3–M4) was substituted for α1 from Arg313 to Ser390, and the linker sequence SQPARAA was substituted for β3 from Gly308 to Asn421to increase expression[10]. These constructs were cloned into the pHLsec vector[34]

between the N-terminal secretion signal sequence either a double stop codon (for β3) or a C-terminal 1D4 purification tag (for α1). The expression and purification procedure was as described for $\alpha5_{TMD}$ but with the following differences: plasmids encoding the α1 and β3 subunits were cotransfected in a 1:1 ratio, the detergent used for solubilization was decyl maltose neopentyl glycol (DMNG, Anatrace) supplemented with cholesterol hemisuccinate (CHS, Anatrace) at a 10:1 molar ratio, the 15-ml eluted samples were loaded in 5-ml batches onto a Superdex 200 16/600 column (GE Healthcare) equilibrated in 10 mM HEPES, pH 7.2, 150 mM NaCl, 0.007% (w/v) DMNG10:1CHS and 50 μM GABA. Peak fraction concentrations were typically 0.1 mg/ml and were further concentrated by ultrafiltration to 1 mg/ml using 100-kDa-cutoff membranes (Millipore), aliquoted and snap frozen at −80 °C. The final α1β3 $GABA_AR$ yield was 0.05 mg per liter of suspension culture (10g cell pellet).

Nanobody generation and purification. Camelid nanobodies against α1β3 $GABA_ARs$ were generated using established protocols[41]. One animal was immunized six times with the recombinant 1D4-tagged human α1β3 $GABA_AR$ pentamer (described above). Subsequent to library generation, nanobodies were selected by phage display in two different ways: either by passive absorption of the $GABA_A$-α1β3 pentamer or by trapping the receptor using the 1D4 antibody. After two rounds of selections, 96 clones were screened and positive clones were sequenced, revealing 13 nanobody families. The nanobody Nb25, binding to the $GABA_A$ β3 subunit, was produced and purified in milligram quantities from WK6su⁻ *Escherichia coli* bacteria. Bacteria were transformed with ~200 ng of the nanobody expression plasmid pMESy4 containing the nanobody of interest and selected on Lysogeny broth (LB)-agar plates containing 2% glucose and 100 μg/ml ampicillin. 2–3 colonies were used for preparing a preculture, which was used to inoculate 0.5 L Terrific broth (TB) cultures supplemented with 0.1% glucose, 2 mM $MgCl_2$ and 100 μg/mL ampicillin. Cultures were grown at 37 °C until their OD_{600} reached 0.7, at which point Nb25 expression was induced with 1 mM IPTG. After induction, cells were grown at 28 °C overnight and harvested by centrifugation (20 min, 5,000g). Nanobodies were released from the bacterial periplasm by incubating cell pellets with an osmotic shock buffer containing 0.2 M Tris, pH 8.0, 0.5 mM EDTA and 0.5 M sucrose. The C-terminally His6-tagged Nb25 was purified using nickel affinity chromatography (binding buffer: 50 mM HEPES, pH 7.2, 1 M NaCl, 10 mM imidazole; elution buffer: 50 mM HEPES, pH 7.2, 0.2 M NaCl, 0.5 M imidazole) and then subjected to size-exclusion chromatography on a Superdex 75 16/600 column (GE Healthcare) in 10 mM HEPES, pH 7.2, 150 mM NaCl. Nb25 stocks were concentrated to 5–10 mg/mL, snap frozen in liquid nitrogen and stored at −80 °C.

Crystallization and X-ray data collection. The $\alpha5_{TMD}$ construct contains 15 N-linked glycosylation sites, bringing a considerable extra volume, flexibility and potential occupancy heterogeneity. Therefore, before crystallization, concentrated $\alpha5_{TMD}$ samples, with and without pregnanolone, were incubated with 0.01 mg ml⁻¹ endoglycosidase F1 (ref. 42) for 2 h at room temperature. Sitting-drop vapor diffusion crystallization trials were performed in 96-well Swisssci 3-well crystallization plates (Hampton Research) at three ratios: 200 nL protein plus 100 nL reservoir, 100 nL protein plus 100 nL reservoir, 100 nL protein plus 200 nL reservoir. Drops were dispensed by a Cartesian Technologies robot[43], and plates were maintained at 6.5 °C in a Formulatrix storage and imaging system. Initial crystals grew within 1–7 d in a range of conditions[44] and diffracted up to intermediate resolution (>5 Å). Following additive-based optimization (MemAdvantage, Molecular Dimensions), preg-nanolone-bound $\alpha5_{TMD}$ crystals diffracting to 3.2-Å resolution were grown in 14% poly-ethylene (PEG) 6000, 0.1 M *N*-(2-Acetamido)iminodiacetic acid (ADA), pH 5.6, 7.6 mM 4-Cyclohexyl-1-Butyl-β-D-Maltoside (CYMAL-4) and apo $\alpha5_{TMD}$ crystals diffracting to 3.3-Å resolution were grown in 14% poly-ethylene (PEG) 5000, 0.08 M magnesium acetate, 0.1 M sodium citrate, pH 5.8, 1 mM ethylene glycol tetraacetic acid (EGTA). Crystals were cryo-protected by soaking in reservoir solution supplemented with 30% ethylene glycol and were then flash frozen in liquid nitrogen. Diffraction images of 0.2° oscillation were collected at the Diamond Light Source, beamlines I03 (pregnanolone-bound $\alpha5_{TMD}$, λ = 0.9763 Å) and I04 (apo $\alpha5_{TMD}$, λ = 0.9795 Å) on Pilatus3 6M and Pilatus 6M-F detectors, respectively. X-ray data were indexed, integrated and scaled using the HKL2000 package[45] and merged using Aimless[46,47]. Data collection statistics are shown in **Table 1**.

Structure determination, refinement and analysis. Pregnanolone-bound and apo $\alpha5_{TMD}$ structures were solved by molecular replacement using the human GABA$_A$R-β3$_{cryst}$ homopentamer[10] (PDB 4COF) and the gelsolin nanobody[48] (PDB 2X1Q) as a search model in Phaser[49]. Polypeptide chains were traced using iterative rounds of manual model building in Coot[50] and refinement in Refmac[51] and Phenix[52,53]. Automated X-ray and atomic displacement parameter (ADP) weight optimization and torsion angle noncrystallographic symmetry (NCS) restraints, were applied. The pregnanolone coordinates and geometry restraints were generated using the Grade Web Server (http://grade.globalphasing.org). Diffraction from the apo $\alpha5_{TMD}$ crystal was strongly anisotropic. Ellipsoidal truncation, with resolution limits along the reciprocal cell directions a*, b* and c* being 3.9 Å, 3.8 Å and 3.3 Å, respectively, anisotropic scaling and a negative isotropic B-factor correction (−49.29 Å^2) were performed using the UCLA–DOE Lab Diffraction Anisotropy server (https://services.mbi.ucla.edu/anisoscale/)[54]. Anisotropy correction led to improvements in the electron density map quality and facilitated model building. Both data sets (uncorrected and anisotropy-corrected) were deposited in the Protein Data Bank. The model deposited was refined against the anisotropy-corrected data set, however we also provide refinement statistics against the full (uncorrected) data set in **Table 1**.

The final models contain one $\alpha5_{TMD}$ homopentamer bound to five Nb25 nanobodies per asymmetric unit. The complete polypeptide chains could be built, with the exception of thirteen N-terminal (QSVNDPGNMSFVK) and thirteen C-terminal (NREPVIKGAASPK) GABA$_A$ residues, the final serine residue in nanobody chains L, M and N and the C-terminal purification tags, presumably disordered. Furthermore, very strong additional electron density peaks were clearly visible in the outer parts of intersubunit TMD regions in the $\alpha5_{TMD}$ maps. These could be unambiguously assigned to five pregnanolone molecules, one per intersubunit interface, based on shape, coordination and refinement statistics. The $\alpha5_{TMD}$ extracellular region is heavily glycosylated, and we observed clear electron density for 10 out of the 15 N-linked glycosylation sites, with the remaining five being located in the N-terminal disordered regions. Glycans attached to Asn149 in each chain were protected from endoglycosidase F1 cleavage owing to extensive interactions with both $\alpha5_{TMD}$ and the Nb25 nanobody molecules, underlying their important structural role[10]. Stereochemical properties of the models were assessed in Coot[50] and Molprobity[55]. Protein geometry analyses revealed no Ramachandran outliers, with 97.88% residues in favored regions, 2.12% residues in allowed regions for pregnanolone-bound $\alpha5_{TMD}$ and 96.76% residues in favored regions and 3.24% residues in allowed regions for apo $\alpha5_{TMD}$. The overall Molprobity scores are 1.24 and 1.74, respectively (100th percentile).

Structural alignments were performed in SHP[56]. Protein interfaces were analyzed using the PDBePISA web server at the European Bioinformatics Institute (http://www.ebi.ac.uk/pdbe/prot_int/pistart.html)[57] and pore dimensions were analyzed using the Coot implementation of Hole[58], with a probe radius of 1.4 Å. Structural figures were prepared with the PyMOL Molecular Graphics System, Version 1.8, Schrödinger, LLC. Molecular videos and analyses were performed with the UCSF Chimera package, developed by the Resource for Biocomputing, Visualization, and Informatics at the University of California, San Francisco (supported by NIGMS P41-GM103311) (ref. 59).

Cell preparation and electrophysiology. One day before experiments, 8 mL of DMEM was preincubated for 10 min at room temperature with 96 μL Lipofectamine2000 (Thermofisher) and 48 μg plasmid DNA, then added to a single T175 cm^2 flask containing HEK293T cells (30–50% confluency; HEK 293T, ATCC Cat# CRL-3216, RRID: CVCL_0063) and 2 mL DMEM (supplemented with 10% FCS, L-glutamine and nonessential amino acids). After 3 h, this media was removed and replaced by DMEM supplemented with 10% FCS. For GABA$_A$R heteromers, pHLsec plasmids containing human full-length cDNA constructs were mixed in a 1:1:2 ratio (α:β:γ), supplemented with 3% plasmid encoding enhanced GFP (EGFP) to assess transfection efficiency. Specifically, the cDNA inserts used for heteromeric receptor expression were as follows: human GABA$_A$R α1 mature protein sequence (α1 Uniprot P14867 entry Gln28 is Gln1 1-429 QPSL…PTPHQ) and human β3 mature protein sequence (β3 Uniprot P28472 entry isoform 1 Gln26 is Gln1 1-448 QVSN…LYYVN) cloned into the pHLsec vector[34] between the N-terminal secretion signal sequence and a double stop codon; human GABA$_A$R γ2 mature protein sequence (γ2 Uniprot P18507 isoform 1 entry Gln40 is Gln1 1-428 QKSDD…SYLYL) cloned into the pHLsec vector[34] between the N-terminal secretion signal sequence followed by

streptavidin-binding protein (MDEKTTGWRGGHVVEGLAGELEQLRARLE HHPQGQREP) and a C-terminal 1D4 purification tag. Transfection efficiencies were typically 50–80% (cells expressing EGFP, as estimated by fluorescence microscopy). 18–24 h later, cells were washed with PBS, incubated in 4 ml TrypLE (Gibco) for 7 min at 37 °C, suspended in 21 ml DMEM supplemented with 10% FCS and L-glutamine, centrifuged at 100g for 1.5 min, then suspended in 50 ml Freestyle 293 Expression Medium (Gibco) and placed in a shaking incubator (130 r.p.m., 37°C, 8% CO$_2$) for 30 min. 25 ml of cell suspension was then centrifuged at 100g for 1.5 min and suspended in 4 ml of external recording solution. This solution contained: 137 mM NaCl, 4 mM KCl, 1 mM MgCl$_2$, 1.8 mM CaCl$_2$, 10 mM HEPES and 10 mM D-Glucose, pH 7.4 (≈305 mOsm). The internal recording solution contained: 140 mM CsCl, 5 mM NaCl, 1 mM MgCl$_2$, 10 mM HEPES, 5 mM EGTA, 0.2 mM ATP, pH 7.35 (≈295 mOsm). Electrophysiological recordings were performed at room temperature using an Ionflux16 (Molecular Devices) in ensemble mode, with series resistance compensation set at 80% and cells held at −60 mV. Pregnanolone and allopregnanolone (Sigma-Aldrich) were dissolved in DMSO as 100 mM stocks before dilution in external recording solution. These neurosteroids were coapplied with EC$_{10-15}$ GABA or histamine doses to generate dose–response curves for heteromeric GABA$_A$Rs and $\alpha5_{TMD}$. Expression of heteromeric receptors as assemblies of αβγ subunits was confirmed by response to GABA, which requires coassembly of α1 and β3 subunits, and efficient inclusion of the γ2 subunit into αβγ heteromers was verified by testing for Zn^{2+} sensitivity, with heteromeric constructs exhibiting low sensitivity to Zn^{2+}, defined as less than 50% inhibition of an EC$_{50}$ GABA response[60].

Molecular docking and binding-energy calculation. Small-molecule coordinates were generated by eLBOW and energy minimized with Ligprep in the Schrödinger suite at pH 7.0 with the OPLS_2005 force field[61]. The standard conversion procedure with full hydrogen optimization was applied with the Protein Preparation workflow to the protein structure. The neurosteroid-binding pocket between chains B and C in $\alpha5_{TMD}$ was used for the subsequent grid generation and ligand-docking procedures. The Glide Grid[62,63] (Schrödinger suite) was built using an inner box (the centroid of the pregnanolone molecule) of $10 \times 10 \times 10$ Å^3 and an outer box (within which all the ligand atoms must be contained) that extended 20 Å in each direction from the inner box. Default values were used for all other parameters. The hydrogen bonds between the 3α-hydroxyl group and the 20-carbonyl group of the pregnanolone molecule, respectively, with the carbonyl group of Gln245 and hydroxyl group of Thr309 were used as positional constraints. Furthermore, the atoms C03, C20 and C06 of the pregnanolone molecule were used as additional positional constraints. For docking, the QMPLD[26] protocol (Schrödinger suite, http://www.schrodinger.com/) was used. The most reliable binding pose for each small molecule was selected on the basis of calculated van der Waals and electrostatic interactions. r.m.s. deviation values were calculated with VMD[64].

Thermostability binding experiments. Information regarding the thermostability of a detergent-solubilized protein can be determined by heating protein samples over a range of temperatures for equal time periods and then measuring the reduction in the intensity of the monodisperse SEC profile for each protein sample[65]. With increasing temperature, an increased proportion of protein is denatured, forms aggregates and is lost from the monodisperse peak when the protein is subsequently run on SEC. A measure of protein stability can then be obtained by plotting the decay in peak UV absorbance against increasing temperature, for example to obtain a 50% melting temperature (T_m). Purified GABA$_A$R $\alpha5_{TMD}$ or $\alpha5_{TMD}$ mutants at 0.02 mg ml^{-1} (100 nM) in 150 mM NaCl, 10 mM HEPES, pH 7.2, 0.007% DDTM (w/v) were separated into 50-μl aliquots in PCR tubes and heated at a range of temperatures from 40–80 °C for 1 h. Samples were run on a high-performance liquid chromatography system with an automated micro-volume loader (Shimadzu) through a Superdex 200 Increase 3.2/300 column (GE Healthcare) maintained in 300 mM NaCl, 10 mM HEPES and 0.007% DDTM (w/v). Monodisperse peak reduction with increasing temperature was measured relative to an unheated control sample maintained at 4 °C.

Importantly, because some drugs thermostabilize when bound to detergent-solubilized protein[65], the thermostability assay offers an efficient strategy to measure protein sensitivity to drugs in the detergent-solubilized environment. Purified GABA$_A$R $\alpha5_{TMD}$ or $\alpha5_{TMD}$ mutants were separated into PCR tubes, supplemented with pregnanolone at a range of concentrations and heated at Tm30%

(the temperature at which the monodisperse peak was reduced by 70%) for 1 h. Afterward, samples were run on a high-performance liquid chromatography system with an automated micro-volume loader (Shimadzu) through a Superdex 200 3.2/300 column (GE Healthcare) maintained in 300 mM NaCl, 10 mM HEPES and 0.007% DDTM. Drug dose–response curves were generated by plotting UV absorbance against drug concentration.

Cell lines used. HEK293S-GnTI⁻ cells (ATCC Cat# CRL-3022, RRID: CVCL_ A785) and HEK 293T (ATCC Cat# CRL-3216, RRID: CVCL_0063) were both confirmed free from mycoplasma contamination.

Data availability. The atomic coordinates and the structure factors are available from the Protein Data Bank under accession codes PDB 5O8F (pregnanolone-bound $\alpha5_{TMD}$) and PDB 5OJM (apo $\alpha5_{TMD}$). Source data for **Figures 1e**, **3e** and **3f** are available online. A **Life Sciences Reporting Summary** for this article is available.

33. Jansen, M., Bali, M. & Akabas, M.H. Modular design of Cys-loop ligand-gated ion channels: functional 5-HT3 and GABA rho1 receptors lacking the large cytoplasmic M3M4 loop. *J. Gen. Physiol.* **131**, 137–146 (2008).
34. Aricescu, A.R., Lu, W. & Jones, E.Y. A time- and cost-efficient system for high-level protein production in mammalian cells. *Acta Crystallogr. D Biol. Crystallogr.* **62**, 1243–1250 (2006).
35. Molday, R.S. & MacKenzie, D. Monoclonal antibodies to rhodopsin: characterization, cross-reactivity, and application as structural probes. *Biochemistry* **22**, 653–660 (1983).
36. Oprian, D.D., Molday, R.S., Kaufman, R.J. & Khorana, H.G. Expression of a synthetic bovine rhodopsin gene in monkey kidney cells. *Proc. Natl. Acad. Sci. USA* **84**, 8874–8878 (1987).
37. Reeves, P.J., Callewaert, N., Contreras, R. & Khorana, H.G. Structure and function in rhodopsin: high-level expression of rhodopsin with restricted and homogeneous N-glycosylation by a tetracycline-inducible N-acetylglucosaminyltransferase I-negative HEK293S stable mammalian cell line. *Proc. Natl. Acad. Sci. USA* **99**, 13419–13424 (2002).
38. Aricescu, A.R. & Owens, R.J. Expression of recombinant glycoproteins in mammalian cells: towards an integrative approach to structural biology. *Curr. Opin. Struct. Biol.* **23**, 345–356 (2013).
39. Zacharias, D.A., Violin, J.D., Newton, A.C. & Tsien, R.Y. Partitioning of lipid-modified monomeric GFPs into membrane microdomains of live cells. *Science* **296**, 913–916 (2002).
40. Nagai, T. *et al.* A variant of yellow fluorescent protein with fast and efficient maturation for cell-biological applications. *Nat. Biotechnol.* **20**, 87–90 (2002).
41. Pardon, E. *et al.* A general protocol for the generation of Nanobodies for structural biology. *Nat. Protoc.* **9**, 674–693 (2014).
42. Chang, V.T. *et al.* Glycoprotein structural genomics: solving the glycosylation problem. *Structure* **15**, 267–273 (2007).
43. Walter, T.S. *et al.* A procedure for setting up high-throughput nanolitre crystallization experiments. Crystallization workflow for initial screening, automated storage, imaging and optimization. *Acta Crystallogr. D Biol. Crystallogr.* **61**, 651–657 (2005).
44. Parker, J.L. & Newstead, S. Current trends in α-helical membrane protein crystallization: an update. *Protein Sci.* **21**, 1358–1365 (2012).
45. Otwinowski, Z. & Minor, W. Processing of X-ray diffraction data collected in oscillation mode. *Methods Enzymol.* **276**, 307–326 (1997).
46. Winn, M.D. *et al.* Overview of the CCP4 suite and current developments. *Acta Crystallogr. D Biol. Crystallogr.* **67**, 235–242 (2011).
47. Evans, P.R. & Murshudov, G.N. How good are my data and what is the resolution? *Acta Crystallogr. D Biol. Crystallogr.* **69**, 1204–1214 (2013).
48. Van den Abbeele, A. *et al.* A llama-derived gelsolin single-domain antibody blocks gelsolin-G-actin interaction. *Cell. Mol. Life Sci.* **67**, 1519–1535 (2010).
49. McCoy, A.J. *et al.* Phaser crystallographic software. *J. Appl. Crystallogr.* **40**, 658–674 (2007).
50. Emsley, P., Lohkamp, B., Scott, W.G. & Cowtan, K. Features and development of Coot. *Acta Crystallogr. D Biol. Crystallogr.* **66**, 486–501 (2010).
51. Murshudov, G.N. *et al.* REFMAC5 for the refinement of macromolecular crystal structures. *Acta Crystallogr. D Biol. Crystallogr.* **67**, 355–367 (2011).
52. Adams, P.D. *et al.* PHENIX: a comprehensive Python-based system for macromolecular structure solution. *Acta Crystallogr. D Biol. Crystallogr.* **66**, 213–221 (2010).
53. Afonine, P.V. *et al.* Towards automated crystallographic structure refinement with phenix.refine. *Acta Crystallogr. D Biol. Crystallogr.* **68**, 352–367 (2012).
54. Strong, M. *et al.* Toward the structural genomics of complexes: crystal structure of a PE/PPE protein complex from Mycobacterium tuberculosis. *Proc. Natl. Acad. Sci. USA* **103**, 8060–8065 (2006).
55. Chen, V.B. *et al.* MolProbity: all-atom structure validation for macromolecular crystallography. *Acta Crystallogr. D Biol. Crystallogr.* **66**, 12–21 (2010).
56. Stuart, D.I., Levine, M., Muirhead, H. & Stammers, D.K. Crystal structure of cat muscle pyruvate kinase at a resolution of 2.6 A. *J. Mol. Biol.* **134**, 109–142 (1979).
57. Krissinel, E. & Henrick, K. Inference of macromolecular assemblies from crystalline state. *J. Mol. Biol.* **372**, 774–797 (2007).
58. Smart, O.S., Goodfellow, J.M. & Wallace, B.A. The pore dimensions of gramicidin A. *Biophys. J.* **65**, 2455–2460 (1993).
59. Pettersen, E.F. *et al.* UCSF Chimera–a visualization system for exploratory research and analysis. *J. Comput. Chem.* **25**, 1605–1612 (2004).
60. Hosie, A.M., Dunne, E.L., Harvey, R.J. & Smart, T.G. Zinc-mediated inhibition of GABA(A) receptors: discrete binding sites underlie subtype specificity. *Nat. Neurosci.* **6**, 362–369 (2003).
61. Banks, J.L. *et al.* Integrated modeling program, applied chemical theory (IMPACT). *J. Comput. Chem.* **26**, 1752–1780 (2005).
62. Friesner, R.A. *et al.* Glide: a new approach for rapid, accurate docking and scoring. 1. Method and assessment of docking accuracy. *J. Med. Chem.* **47**, 1739–1749 (2004).
63. Halgren, T.A. *et al.* Glide: a new approach for rapid, accurate docking and scoring. 2. Enrichment factors in database screening. *J. Med. Chem.* **47**, 1750–1759 (2004).
64. Humphrey, W., Dalke, A. & Schulten, K. VMD: visual molecular dynamics. *J. Mol. Graph.* **14**, 33–38 (1996).
65. Hattori, M., Hibbs, R.E. & Gouaux, E. A fluorescence-detection size-exclusion chromatography-based thermostability assay for membrane protein precrystallization screening. *Structure* **20**, 1293–1299 (2012).

natureresearch

Corresponding Author: Radu Aricescu

Date: Jul 26, 2017

Life Sciences Reporting Summary

Nature Research wishes to improve the reproducibility of the work we publish. This form is published with all life science papers and is intended to promote consistency and transparency in reporting. All life sciences submissions use this form; while some list items might not apply to an individual manuscript, all fields must be completed for clarity.

For further information on the points included in this form, see Reporting Life Sciences Research. For further information on Nature Research policies, including our data availability policy, see Authors & Referees and the Editorial Policy Checklist.

▶ Experimental design

1. Sample size

   Describe how sample size was determined.

   > Electrophysiology experiments were performed minimally in triplicate, as described in the methods and figure legends. Crystallography experiments relied on single crystals (for both apo and neurosteroid-bound forms), however these provide sufficient internal redundancy.

2. Data exclusions

   Describe any data exclusions.

   > Diffraction from the apo α5TMD crystal was strongly anisotropic. Ellipsoidal truncation, with resolution limits along the reciprocal cell directions a*, b* and c* being 3.9 Å, 3.8 Å and 3.3 Å respectively, anisotropic scaling and a negative isotropic B-factor correction (-49.29 Å^2) were performed using the UCLA-DOE Lab Diffraction Anisotropy server (https://services.mbi.ucla.edu/anisoscale/). Anisotropic correction led to improvements in the electron density map quality and facilitated model building. The model deposited was refined against the truncated dataset, however we have also deposited the full dataset and provide refinement statistics against it in Table 1.

3. Replication

   Describe whether the experimental findings were reliably reproduced.

   > All functional experiments were repeated (minimal n=3) and results were consistent. Error bars etc are provided.

4. Randomization

   Describe how samples/organisms/participants were allocated into experimental groups.

   > Samples were not randomized.

5. Blinding

   Describe whether the investigators were blinded to group allocation during data collection and/or analysis.

   > Not applicable.

   Note: all studies involving animals and/or human research participants must disclose whether blinding and randomization were used.

6. Statistical parameters

For all figures and tables that use statistical methods, confirm that the following items are present in relevant figure legends (or the Methods section if additional space is needed).

n/a	Confirmed	
☐	☒	The <u>exact</u> sample size (*n*) for each experimental group/condition, given as a discrete number and unit of measurement (animals, litters, cultures, etc.)
☐	☒	A description of how samples were collected, noting whether measurements were taken from distinct samples or whether the same sample was measured repeatedly.
☐	☒	A statement indicating how many times each experiment was replicated
☐	☒	The statistical test(s) used and whether they are one- or two-sided (note: only common tests should be described solely by name; more complex techniques should be described in the Methods section)
☒	☐	A description of any assumptions or corrections, such as an adjustment for multiple comparisons
☒	☐	The test results (e.g. *p* values) given as exact values whenever possible and with confidence intervals noted
☒	☐	A summary of the descriptive statistics, including central tendency (e.g. median, mean) and variation (e.g. standard deviation, interquartile range)
☐	☒	Clearly defined error bars

See the web collection on statistics for biologists for further resources and guidance.

▶ Software

Policy information about availability of computer code

7. Software

Describe the software used to analyze the data in this study.

> HKL2000 (X-ray data indexing, integrating, scaling); Aimless (merging); Phaser (molecular replacement); Coot (model building); Refmac, Phenix (model refinement); Grade (pregnanolone geometry restraints generation); UCLA-DOE Lab Diffraction Anisotropy server (anisotropy correction); Molprobity (model quality control); SHP (structural alignments); PDBePISA (protein interface analyses); Hole (channel pore analysis); Pymol (figure generation); UCSF Chimera (movie generation); Schrödinger suite packages (molecular docking); IonFlux Data Analyzer 4 (electrophysiology data collection and processing); OriginPro (graph generation).

For all studies, we encourage code deposition in a community repository (e.g. GitHub). Authors must make computer code available to editors and reviewers upon request. The *Nature Methods* guidance for providing algorithms and software for publication may be useful for any submission.

▶ Materials and reagents

Policy information about availability of materials

8. Materials availability

Indicate whether there are restrictions on availability of unique materials or if these materials are only available for distribution by a for-profit company.

> There is no restriction, other than customary MTA arrangements required by academic institutions.

9. Antibodies

Describe the antibodies used and how they were validated for use in the system under study (i.e. assay and species).

> Rho-1D4 antibody (purchased from the University of British Columbia), for affinity protein purification (extensively used in the literature over several decades). Nanobody 25 against human beta3 GABAA receptor subunit, raised in llamas for this study. Binding confirmed by surface plasmon resonance and crystallography.

10. Eukaryotic cell lines

    a. State the source of each eukaryotic cell line used.

> HEK293S-GnTI- cells (ATCC Cat# CRL-3022, RRID: CVCL_A785), for protein production;
> HEK 293T (ATCC Cat# CRL-3216, RRID: CVCL_0063), for electrophysiology experiments.

    b. Describe the method of cell line authentication used.

> Cell lines were purchased from the ATCC.

    c. Report whether the cell lines were tested for mycoplasma contamination.

> Cell lines were tested and confirmed free from mycoplasma contamination.

    d. If any of the cell lines used in the paper are listed in the database of commonly misidentified cell lines maintained by ICLAC, provide a scientific rationale for their use.

> Not applicable.

▶ Animals and human research participants

Policy information about studies involving animals; when reporting animal research, follow the ARRIVE guidelines

11. Description of research animals

    Provide details on animals and/or animal-derived materials used in the study.

> Not applicable.

Policy information about studies involving human research participants

12. Description of human research participants

    Describe the covariate-relevant population characteristics of the human research participants.

> Not applicable.